ingegneria sismica
International Journal of Earthquake Engineering
Anno XLIII - Num. 3 - 2026

Modeling of Smartphone Battery State of Charge and Power Consumption Patterns Based on a Multi-Physics Coupled State-Space Model

Yuchen Yang[1,*], *Zichen Xue*[2] *and Shiyan Jiang*[1]

[1] School of Science, Nanjing University of Posts and Telecommunications, Nanjing, China, 210023

[2] Portland Institute, Nanjing University of Posts and Telecommunications, Nanjing, China, 210023

SUMMARY: *To address the complex nonlinear characteristics of smartphone battery power consumption, this paper constructs a continuous-time state-space framework that integrates multiple physics, aiming to achieve accurate predictions of battery state of charge and remaining runtime. The research framework consists of a nested structure comprising a fast-time-scale dynamic layer and a slow-time-scale reduced-order layer: the fast-time-scale layer utilizes an improved Thevenin equivalent circuit to capture transient current and voltage responses as well as thermal accumulation processes; the slow-time-scale layer dynamically corrects for battery capacity degradation and internal resistance changes based on the Arrhenius law and cycling history. The study conducted an in-depth analysis of power consumption mechanisms at the hardware level and established a refined power consumption model that incorporates screen pixel brightness, dynamic processor frequency scaling, network connection protocol status, and GPS signal coupling. By iteratively solving a system of nonlinear ordinary differential equations using the fourth-order Runge-Kutta algorithm, this paper conducted simulation validations across various real-world scenarios, including gaming, social media, 4K video, and voice calls. The results indicate that high-load tasks such as gaming significantly shorten battery life due to peak network and processor loads, and that low-temperature environments and health degradation have a significant negative coupling effect on battery life. Sensitivity analysis further reveals that the battery's rated capacity and high-brightness screen loads are the core drivers affecting battery life. This study provides important theoretical support and practical recommendations for optimizing energy management systems in mobile devices.*

KEYWORDS: *Continuous-time modeling, battery state-of-charge prediction, state-space framework.*

1 Introduction

Smartphones have become essential tools in modern life, yet the unpredictability of their battery behavior remains a critical bottleneck in technological development. Due to the interplay of hardware load, thermodynamic dynamics, and electrochemical aging, battery power consumption exhibits complex nonlinear characteristics. Traditional battery life predictions often rely on a simple model of battery capacity divided by power consumption,

*b23090406@njupt.edu.cn
https://doi.org/10.65102/is20261272 Published: 10 June, 2026

neglecting the real-time impact of temperature fluctuations, cycle life, and hardware transient responses on power consumption. This leads to frequent instances of unexpected shutdown anxiety among users due to inaccurate battery level indications during actual use. Existing research on battery power consumption has primarily focused on either hardware power consumption characteristics or electrochemical degradation mechanisms in isolation, with modeling methods predominantly relying on statistical regression or black-box machine learning[1-3]. However, these methods either exhibit poor generalization capabilities or fail to simultaneously account for both transient load responses and long-term aging degradation characteristics. To address this, this study proposes a nested two-layer state-space modeling scheme that innovatively integrates fast-scale circuit-thermal coupling dynamics with slow-scale electrochemical degradation mechanisms. Based on real-world datasets such as AndroWatts, the study establishes a refined power coupling model that accounts for screen APL intensity, processor DVFS regulation, and the tail effects of network RRC protocols. This approach first characterizes the dynamic evolution of SOC by establishing a system of nonlinear ordinary differential equations, followed by parameter calibration using high-fidelity experimental data from sources such as the NASA PCoE. Finally, numerical integration techniques are employed to predict battery life performance under various complex load scenarios, and multidimensional sensitivity analysis is conducted to identify key drivers of power consumption[4-6].

2 Coupled Multi-physics State-Space SOC Model

In the smartphone's continuous-time SOC model, instead of treating the battery as a simple energy storage container, we model it as a highly sophisticated integrated dynamic system that accounts for electrical, thermal, and electrochemical characteristics. To balance transient task responses with long- term degradation characteristics, we develop a Coupled Multi-Physics State-Space SOC Model[7]. The model comprises two complementary timescales: a Fast-Dynamics layer that captures second- level current transients, voltage responses, and thermal accumulation, serving as the direct basis for Time-to-Empty (TTE) prediction; and a Slow-Dynamics layer that tracks aging effects accumulated through cycling to dynamically calibrate the battery's physical parameters, ensuring model consistency throughout the device's entire lifecycle.

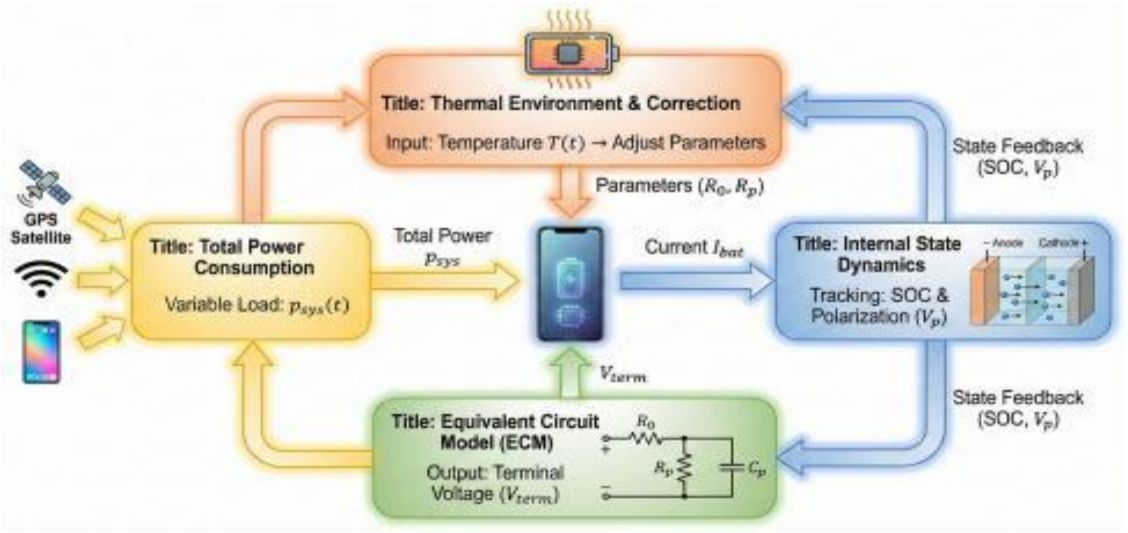

Figure 1: Overall flowchart of our model

Overall flowchart of our model is shown in Figure 1.

2.1 Time-Continuous Dynamics of SOC

For SOC estimation, we utilize an enhanced Equivalent Circuit Model (ECM). By selectively integrating conventional Coulomb counting and a rate-dependent SOC evolution model tailored to diverse operating scenarios, we ultimately derive a refined SOC evolution equation[8, 9].

2.1.1 The Basic Energy Balance Model

The Physical Definition of State of Charge (SOC)

According to the problem statement, the State of Charge (SOC) is defined as the ratio of the current residual deliverable charge to the battery's maximum available capacity under its present condition. Mathematically, it is expressed as:

$$SOC(t) = \frac{Q_{remain}(t)}{Q_{max}} \times 100\% \tag{1}$$

where Qremain(t) denotes the effective residual charge within the battery at time t that is available to the external circuit (measured in Ah or Coulombs). Qmax represents the total deliverable charge when the battery is discharged from a fully charged state to the cut-off voltage, given the current State of Health (SOH) and ambient conditions (measured in Ah or Coulombs)[10-12].

Conventional Coulomb Counting Method the change in the battery's residual charge Qremain(t) is equivalent to the total charge flowed out of the battery. Under the "positive-for-discharge" convention, the relationship between the infinitesimal charge outflow and the current dqout and the current Ibat(t) is expressed as:

$$dQremain(t) = \_\_dqout = \_\_Ibat(t).\ dt \tag{2}$$

Expressed in differential form:

$$\frac{dQ_{remain}(t)}{dt} = -\ I_{bat}(t) \tag{3}$$

Combining the above with the SOC definition:

$$\frac{dSOC}{dt} = \frac{d}{dt}\left(\frac{Q_{remain}}{Q_{mqx}}\right) = \frac{1}{Q_{max}} \cdot \frac{dQ_{remain}(t)}{dt} = -\frac{I_{bat}(t)}{Q_{max}} \tag{4}$$

where Qnom denotes the nominal capacity of the battery (measured in Ah). Assuming the battery voltage remains constant at Vnom, and the total system power is Ptotal(t) the current can be approximated as:

$$I(t) \approx \frac{P_{total}(t)}{V_{nom}} \tag{5}$$

2.1.2 Rate-Effect-Compensated SOC Equation

Physical Current vs. Effective Current

From a physical perspective, the real-time current measured by the sensor is denoted as Ibat(t). In the idealized model, the rate of depletion of the SOC is assumed to be linearly proportional solely to this physical current. In practical electrochemical systems, however, the depletion of the internal state of charge (SOC) often occurs more rapidly than the linear accumulation of the physical current would suggest[13-15].

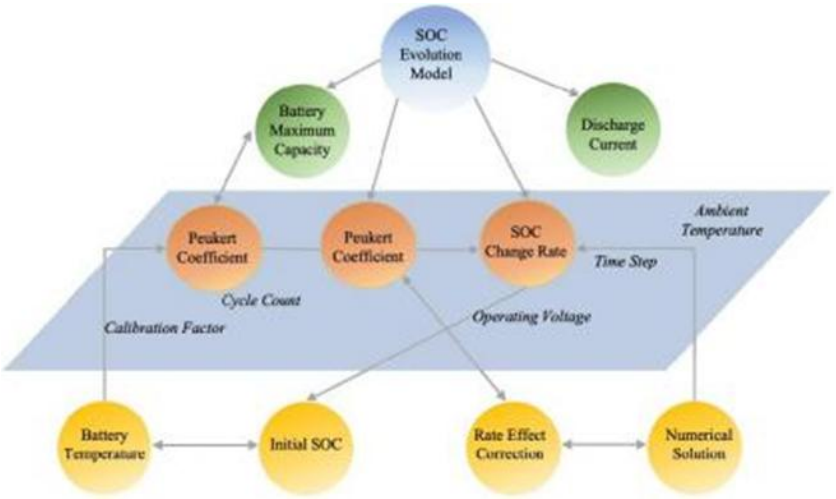

Figure 2: SOC model

SOC model is shown in Figure 2.

To this end, we define the Effective Consumption Current Ieff(t), which represents the equivalent discharge rate perceived by the battery under the prevailing C-rate. The relationship between the two is established via the variable Coulombic efficiency ηc :

$$I_{eff}(t) = \frac{I_{bat}(t)}{\eta_c(I)} \tag{6}$$

Here, the current Ibat(t) follows the "positive-for-discharge" convention. Under high-rate discharge conditions, the effective current Ieff(t) exceeds the physical current Ibat(t), thereby mathematically capturing the accelerated depletion of the SOC[16-18].

Deriving the Rate-dependent Coulombic Efficiency ηc (I) via Peukert's Law

In accordance with the classical Peukert's Law, the efficiency coefficient ηc (I) is treated as a function of discharge intensity rather than a constant value:

$$\eta_c(I) = \left(\frac{I_{ref}}{I_{bat}(t)}\right)^{\epsilon} \tag{7}$$

where Iref(t) denotes the reference current, typically defined as the rated discharge current of the battery (e.g., 1C or C/20). ϵ represents the Peukert-related correction factor. This coefficient is intrinsically linked to the battery's chemical composition and typically satisfies $\epsilon > 0$.

Refined Time-Dynamics SOC Equation

Although Qmax is assumed to be constant at the instant of derivation, the BMS must dynamically update this parameter in practical applications to reflect the influences of ambient environment and battery health. Consequently, the denominator Qmax in the formulation is explicitly defined as a function of temperature T and cycle number k,

representing the aging factor, denoted as Qmax(T, k). Accordingly, the preceding equation is revised as follows:

$$\frac{dSOC(t)}{dt} = -\frac{I_{eff}(t)}{Q_{max}(T,k)} \tag{8}$$

By incorporating the maximum usable capacity of the battery Qmax(T, k), we establish the following ordinary differential equation governing the SOC evolution:

$$\frac{dSOC(t)}{dt} = -\frac{I_{bat}(t)}{\eta_c(I) \cdot Q_{max}(T,k)} \tag{9}$$

2.2 The Improvement of Continuous-Time Model

The assumption of constant voltage overlooks essential voltage dynamics; in practice, the terminal voltage declines as SOC depletes, which necessitates a nonlinear compensatory surge in current to maintain a constant power output[19, 20].

2.2.1 Component-Level Power Modeling

In physics, mobile phone energy consumption refers to total energy used, with specific energy consumption being a key indicator of energy use level and energy-saving performance. Power consumption denotes energy use per unit time (i.e., power loss), defined as the difference between input and output power of devices. For computers and mobile phones—whose processors, memory, and storage are based on CMOS digital integrated circuits—energy consumption typically refers to electrical energy consumed during operation. To establish a coupled model for the total instantaneous power consumption of a mobile phone psys(t) over a given period [0, t], we analyzed the correlation between sub-power components and derived the following correlation matrix using experimental data:

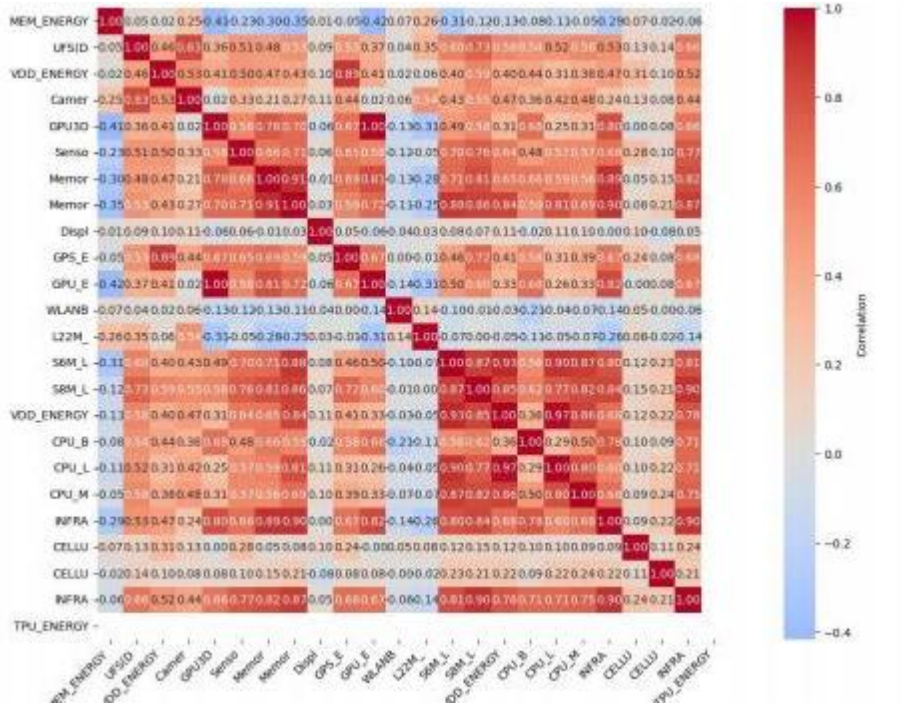

Figure 3: Sub-power correlation matrix

Sub-power correlation matrix is shown in Figure 3.

Based on the correlations between various powers, we selected four strongly correlated sub- powers: screen power consumption p_{screen}, processor power p_{cpu}, network connection power p_{net}, and GPS power P_{gps}.

$$\begin{cases} p_{sys}(t) = \omega_{screen}\phi_{screen} + \omega_{cpu}\phi_{cpu} + \omega_{net}\phi_{net} + \beta\left(\phi_{cpu} \cdot \phi_{net}\right) + \sigma\Delta T \\ \dfrac{dT}{dt} = \dfrac{1}{C_{th}}\left[\gamma p_{sys}(t) - hA(T - T_{amb})\right] \\ \dfrac{dSOH}{dt} = -\,k_{age} \cdot \left(\dfrac{p_{sys}}{p_{std}}\right)^{n} \cdot \exp\left(-\dfrac{E_a}{RT}\right) \end{cases} \tag{10}$$

where $\phi_i = \frac{\partial p_{sys}}{\partial p_i}$ i=screen/cpu/net/gps, pstd is the standard reference power (2000 mW), and the other Greek letters are the coupling coefficients corresponding to each component.

The following are the physical meanings and calculation methods of each sub-power:

(1) Screen Power Consumption

Initially, we attempted to construct the most intuitive model based on the heuristic that higher screen brightness directly correlates with increased power consumption. Specifically, we hypothesized a linear relationship between screen power pscreen(t) and brightness intensity L(t) (0<L(t)<1), formulated as: pscreen(t) = α + β. L(t).

However, empirical validation yielded a coefficient of determination (R2) of only 0.46, indicating that brightness alone is an insufficient predictor. Further analysis reveals that display content (color depth) significantly modulates power, necessitating the introduction of the Average Picture Level (APL). APL represents the mean pixel intensity—ranging from 0 (all-black) to 1 (all-white)—and is derived from RGB channel data as follows:

$$APL = \frac{1}{3} \times \left(\frac{R}{255} + \frac{G}{255} + \frac{B}{255}\right) \tag{11}$$

We finally refined the model into the following formulation:

$$p_{screen}(t) = p_{static} + p_{max}.\ L(t).\ APL(t) \tag{12}$$

In this formulation, pstatic represents the static baseline power of the screen—the energy consumed as long as the display is active, regardless of content. pmax denotes the maximum dynamic power, which corresponds to the energy required for all OLED sub-pixels to emit light at full intensity. This model explicitly accounts for why "Dark Mode" significantly reduces energy consumption.

(2) CPU Power Consumption

Literature review indicates that core smartphone chips are almost entirely composed of Complementary Metal-Oxide-Semiconductor (CMOS) circuits. Physically, the dynamic power consumption of CMOS circuits primarily originates from the charging and discharging of load capacitance during logic state transitions, where the energy stored in the capacitor is $E = \frac{1}{2}$ cV2.

Since power represents energy consumption per unit time, assuming a clock frequency f and an average switching probability (activity factor) α per cycle, the dynamic power consumption is formulated as: pdynamic = α. c. V2. f

In practical engineering, however, increasing the clock frequency f shortens the signal propagation time between logic gates. To ensure that transistors complete their state

transitions within this reduced time frame, the driving voltage (DVFS) V must be elevated. To maintain timing stability, the voltage V is required to increase linearly with the frequency f:

$$p_{dynamic} \alpha f. V2 \alpha f. f2 = f3 \quad (13)$$

This implies a cubic relationship between power pdynamic and frequency f, which explains the exponential surge in heat generation and power consumption during high-frequency operations, such as intensive gaming.

(3) Network Connectivity

Unlike the screen or CPU, cellular network energy consumption does not scale linearly with the volume of transmitted data (MB). Instead, it is governed by the communication protocol's "states." To minimize latency, telecommunication operators employ the Radio Resource Control (RRC) protocol. This ensures that the network hardware does not shut down immediately after data transmission; instead, it enters a high-power maintenance period.

To mathematically characterize this non-linear behavior, we establish a piecewise constant model:

$$p_{net}(t) = \begin{cases} p_{idle} & \text{state} = \text{IDLE} \\ p_{high} & \text{state} = \text{TX/RX} \\ p_{tail} & \text{state} = \text{TAIL} \end{cases} \quad (14)$$

DCH (Active State): When users are actively downloading or uploading data, the power amplifier (PA) operates at full capacity, leading to peak power consumption phigh.

TAIL (Tail State): This is the pivotal highlight of our model. Upon the conclusion of data transmission (Data =0), the system does not immediately transition to sleep; instead, it enters a "tail state" that persists for approximately 10 to 15 seconds. During this interval, despite the absence of data traffic, the hardware remains in high-power ptail standby.

IDLE (Sleep State): Only after the inactivity timer expires does the system revert to low-power mode pidle, maintaining only essential "heartbeat" packets for connectivity.

This explains why frequent bursts of small messages consume more power than continuous large- scale downloads: the former triggers multiple instances of inefficient high-power 'tails'.

(4) GPS and Signal Coupling

Unlike the previously discussed power logic, a GPS receiver's energy consumption is intrinsically driven by computational complexity. The GPS chip must perform a 'statistical search' to extract faint satellite signals from thermal noise under conditions of extremely low Signal-to-Noise Ratio (SNR). To quantify the nonlinear impact of ambient signal quality on power consumption, and drawing upon existing literature, we establish the following coupling model:

$$p_{gps}(t) = \delta_{gps}(t). (p_{track} + p_{search}. e^{-\lambda.SNR(t)}) \quad (15)$$

Specifically, δgps(t) represents whether the user has enabled the GPS function, acting as a discrete binary variable restricted to values of 0 or 1. λ is the sensitivity attenuation factor, reflecting the chip algorithm's resilience against weak signals; a more advanced process technology typically results in a smaller λ. The term e__λ.SNR(t) represents the environmental coupling component: as SNR approaches 0 (indicating extremely poor signal quality), e__λ.SNR(t) tends toward 1, causing the search power consumption to reach its maximum, psearch; conversely, when SNR is high, e__λ.SNR(t) approaches 0, and power consumption returns to the baseline level.

2.2.2 Circuit Dynamics and Current Solving

We model the battery as a first-order Thevenin equivalent circuit, which effectively captures the voltage hysteresis effect.

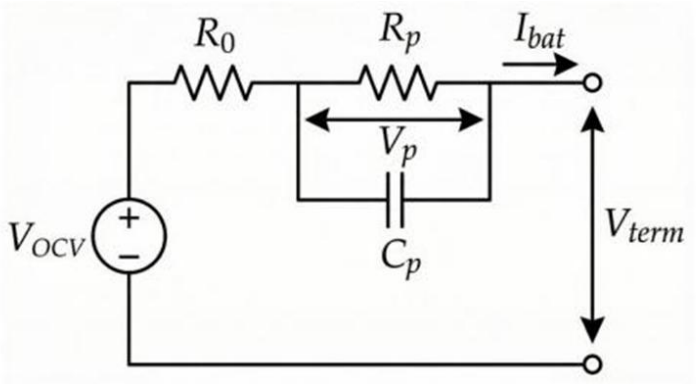

Figure 4: Thevenin equivalent circuit

Thevenin equivalent circuit is shown in Figure 4.

(1) Circuit State Equation

The terminal voltage Vterm is composed of open-circuit voltage VOCV, polarization voltage Vp, and ohmic voltage drop Ibat(t)R0 :

$$\text{Vterm}(t) = \text{VOCV}(\text{SOC}) \_\_ \text{Vp}\,(t) \_\_ \text{Ibat}(t)\text{R0}\,(\text{T}) \tag{16}$$

where the polarization voltage Vp obeys the following differential equation:

$$\frac{dV_p(t)}{dt} = \frac{I_{bat}(t)}{C_p} - \frac{V_p(t)}{R_pC_p} \tag{17}$$

where Rp denotes the polarization resistance, Cp represents the polarization capacitance, and RpCp = τ is the polarization time constant (s).

(2) Current Calculation

Combined with the power balance equation psys/η = Vterm. Ibat, we derive a quadratic equation in terms of Ibat:

$$\text{R0}.\ \text{Ibat}^2 \_\_ (\text{VOCV} \_\_ \text{Vp}\ ).\ \text{Ibat} + \text{psys}/\eta = 0 \tag{18}$$

When solving this equation, to ensure physical consistency with the discharge process, we select the smaller real root, which is expressed as:

$$I_{bat}(t) = \frac{(V_{OCV} - V_p) - \sqrt{(V_{OCV} - V_p)^2 - 4R_0(p_{sys}/\eta)}}{2R_0} \tag{19}$$

Substituting the SOC state equation into the expression for I_{bat} yields:

$$\frac{dSOC(t)}{dt} = -\frac{1}{Q_{max}} \cdot \frac{V_{OCV} - \sqrt{V_{OCV}^2 - 4R_0(p_{sys}/\eta)}}{2R_0} \tag{20}$$

2.3 The Comprehensive Dual-Layer Coupled System

After solving the actual current problem through physical analysis, we modified the model to reflect the dynamic evolution of battery parameters driven by temperature fluctuations and cycling history; To further incorporate environmental temperature and battery aging factors, the model will be upgraded to a double-layer structure. While the first layer deals with fast-scale dynamics, the second layer introduces parametric drift driven by temperature and cycle life, operating on a slower manifold.

2.3.1 Layer 1: Fast Dynamics (Continuous-Time with Thermal Loop)

a) Differential equation of Heat Generation

We assume that the internal thermal conductivity of the battery is extremely high and the temperature distribution is uniform, so we consider it as a uniform thermal mass point. This allows us to simplify complex thermodynamic partial differential equations into ordinary differential equations (ODE) with respect to time. Based on the law of conservation of energy, the real-time temperature change of the battery follows the following dynamic equation:

$$C_{th}\frac{dT(t)}{dt} = p_{gen}(t) - p_{diss} \tag{21}$$

where the heat generation term pgen is denoted as Joule heat generated by the battery while the heat dissipation term pdiss follows Newton's law of cooling.

b) Internal resistance

The most dynamic parameter in the model is internal resistance R0 (T). Under low temperature conditions, the internal resistance increases exponentially according to the Arrhenius relationship. This creates a positive feedback loop: low temperature leads to high internal resistance, which generates more Joule heat, which in turn heats the battery and gradually reduces the internal resistance.

$$R_0(T) = A \cdot \exp\left(\frac{E_a}{R_g T}\right) \tag{22}$$

where A refers to the pre factor, which is related to the microstructure of the material, Ea denotes activation energy, Rg is a universal gas constant.

2.3.2 Layer 2: Slow Dynamics (Aging & History)

In order to consider the structural degradation of batteries during long-term usage, we established a slow dynamic layer model. By tracking the chemical damage caused by discharge cycles, a regularly corrected parameter benchmark is provided for the fast dynamic layer created above, enabling equations to adapt to the complete process of battery changes from "new" to "aging". We mainly consider the impact on the remaining charge Qremain and battery impedance R.

a) Remaining charge

According to literature review, traditional empirical models often assume that battery degradation is linear and ignore the nonlinear disturbance of charging rate (C-rate) on the internal electrochemical environment. It has been found that high C-rate significantly changes the internal structure of the battery, resulting in a significant decrease in available capacity, and the damage rate is directly proportional to SOC. This degradation mode is completely different from that of slow C-rate. Therefore, this sub-model no longer considers the number

of cycles k as a single variable, but instead weights and accumulates the throughput of each charging behavior in ampere hours. Among them, cycles in the high SOC range are assigned higher mechanical damage weights, while charging currents exceeding the threshold are assigned lithium precipitation penalty weights. So we can obtain the mathematical expression of the remaining charge under the degradation mechanism:

$$Qremain(k) = Qnom.\ (1 — Lcal(t) — Lcyc(k, I) — Lplat(I, T)) \quad (23)$$

where Qnom represents the rated capacity of the battery, and Lcal, Lcyc, Lplat are denoted as capacity loss factors ranging from 0 to 1, representing three main aging mechanism below:

Calendar Aging: The diffusion restriction process of ions in the SEI film in the battery leads to the natural growth of the SEI film over time, resulting in a decrease in the available charge capacity.

Cycle History Penalty: The insertion and extraction of lithium ions during battery charging and discharging can cause volume expansion and contraction of electrode particles, leading to particle cracking, especially in the high SOC range (85% -100%), resulting in nonlinear decay of total charge capacity. Among them, ΔQi is the throughput of the second cycle and σ(soc) is a stress weighting function that applies higher damage weights to cycles in the high electricity range.

Fast-Charging Penalty: As shown in figure 5, the high current caused by high C-rate can lead to a decrease in negative electrode potential, induce lithium plating, and result in capacity decay. Among them, Ii is the current rate of the second charge and Icrit is the critical current threshold.

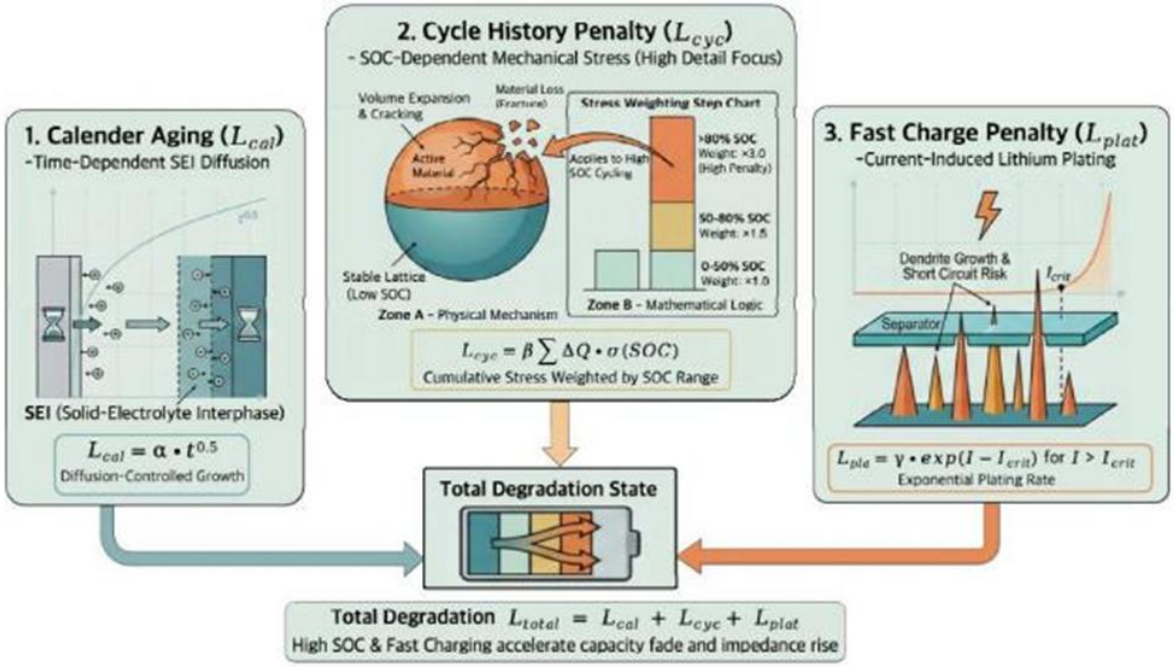

Figure 5: Battery aging loss factors & total degradation

Battery aging loss factors & total degradation is shown in Figure 5.

b) Battery impedance

During the aging process of batteries, impedance not only increases, but also has a "turning point". Based on the literature review, we have obtained the formula (24). From the formula, it can be seen that after fast charging or due to the accumulation of charging cycles

causing the electrolyte to dry out, the impedance will show a nonlinear increase, resulting in a "diving" phenomenon at the end of the battery life.

$$R(k) = R_{initial} \cdot [1 + \mu \cdot L_{cal}(t) + \eta \cdot \left(\frac{Q_{loss}(k)}{Q_{limit}}\right)^{p}] \tag{24}$$

3 SOC Model Extensions

3.1 Battery Depletion Prediction Model

In the formulation of the continuous SOC equation, it is observed that numerous factors—including ambient temperature, battery aging history, and transient power—exert significant influence on battery depletion. To better predict smartphone battery life in real-world scenarios, we have selected the following five representative use cases: Standby Mode, Social Media Browsing, 4K Online Video Streaming, Heavy-load 3D Gaming, Cellular Voice Call (Earpiece Mode).

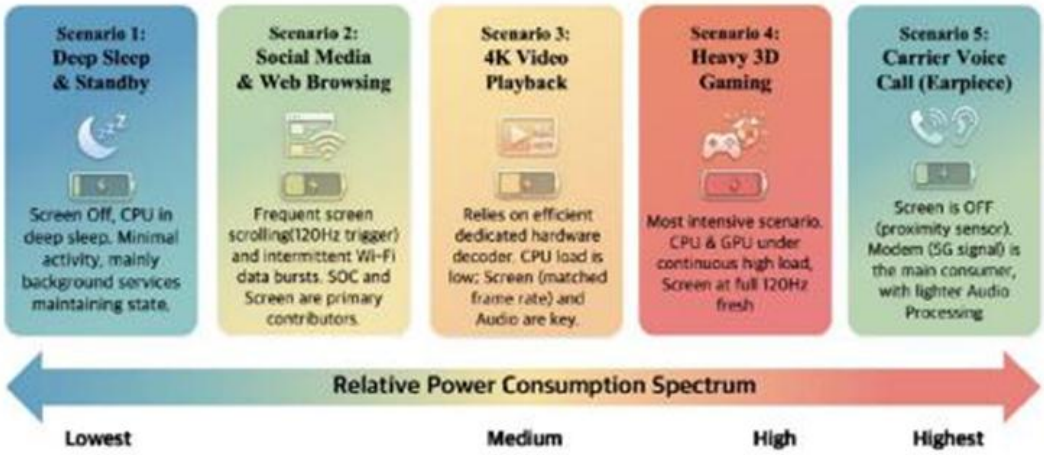

Figure 6: Five scenarios construction

Five scenarios construction is shown in Figure 6.

We perform a logical reformulation of the continuous-time State of Charge (SOC) equation. Based on the reformulated equation and its constituent sub-models, a series of mathematical transformations allows us to derive the relationship between the infinitesimal time element dt and the change in SOC:

$$dt = -\frac{Q_{max}(k,T)V_{ocv}(SOC)}{P_{sys}(t)\left(\frac{I_{bat}}{I_{ref}}\right)^{\varepsilon-1}} dSOC(t) \tag{25}$$

where Qmax denotes the remaining available capacity of the battery. As indicated by the above equation, calculating the total time required for the SOC to drop from its initial state to the cutoff threshold essentially involves the accumulation of infinitesimal time elements corresponding to each incremental change in SOC. By integrating both sides of the equation, we obtain the predictive expression for the Time-to-Exhaust (TTE):

$$TTE = \int_{SOC_{init}}^{SOC_{cutoff}} \frac{Q_{max}(k, T) \cdot V_{ocv}(SOC)}{P_{sys}(t) \cdot \left(\frac{I_{bat}}{I_{ref}}\right)^{\varepsilon-1}} \cdot \frac{1}{100} d(SOC) \quad (26)$$

1

where the coefficient $\frac{1}{100}$ is used to convert the value into a percentage

3.2 Semi-physical Factor Influence Model

By integrating the core parameters from the dual-layer kinetic framework (cycle count, temperature, and charging rate), we establish a simplified semi-physical factor influence model:

SOHdecay=SOH0.exp(__k1.N2__k2.(T__25)2__k3.(Icharge/Icrit)2__k12.N.(T__25))(27)

where SOH0 = 100% represents the initial State of Health, N denotes the number of charge-discharge cycles, and T is the ambient temperature. Icrit = 1c serves as the critical fast-charging current threshold. The parameters k1, k2, and k3 are the influence coefficients for the cycle count, temperature, and charging rate, respectively, while k12 represents the cycle-temperature interaction coefficient.

4 Model Application and Problem Solving

4.1 SOC Model Application: Battery Performance Across Scenarios

4.1.1 Solution Formulas and Parameter Estimation

In this section, we utilize the previously established SOC model to predict battery performance under various usage scenarios. By analyzing the temporal changes in battery state, calculating relevant performance parameters, we evaluate the battery's performance under different conditions.

First, all formulas in the model are presented as follows:

$$\begin{cases} \dfrac{dSOC(t)}{dt} = -\dfrac{I_{eff}(t)}{Q_{max}(N, T)} \\ Q_{max}(N, T) = Q_0 \cdot \left[1 \_\_ k_{cal} \cdot t_{stationary} + \psi_{cyclic} \_\_ \sum_{i=1}^{N} \dfrac{Q_{content}}{RT} \cdot f\left(SOC_{senp,i}\right) + k_{font} \cdot \sum_{i=1}^{N} g\left(I_{charge}\right)\right] \cdot f_T(T) \\ I_{eff}(t) = \dfrac{p_{sys}(t)}{V_{nom}} \left(\dfrac{I_{bat}}{I_{ref}}\right)^{\varepsilon\_1} \\ \begin{cases} p_{sys}(t) = (1)_{screen}\phi_{screen} + (1)_{cpu}\phi_{cpu} + (1)_{net}\phi_{net} + \beta\left(\phi_{cpu} \cdot \phi_{net}\right) + \sigma\Delta T \\ \dfrac{dT}{dt} = \dfrac{1}{C_{th}}\left[\gamma p_{sys}(t) \_\_ h(T \_\_ T_{amb})\right] \end{cases} \\ V_{term} = \_\_ k_{war} \cdot \left(\dfrac{p_{sys}}{T_{amb}}\right)^{\alpha} \cdot \exp\left(\_\_\dfrac{E_a}{RT}\right) \\ V_{term}(t) = V_{ocv}(t) \_\_ I_{bat}(t) \cdot R_0 \_\_ V_p(t) \\ \dfrac{dV_p(t)}{dt} = \dfrac{I_{bat}(t)}{C_p} - \dfrac{V_p(t)}{R_p C_p} \end{cases} \quad (28)$$

We assigned specific coefficients based on the experimental data of smartphone hardware power consumption and electrochemical property from the AndroWatts Mobile Energy

Database and NASA PCoE Battery Aging Database. The revised total power coupling model are as follows:

$$\begin{cases} p_{sys}(t) = 0.42\phi_{screen} + 0.28\phi_{cpu} + 0.15\phi_{net} + 0.22(\phi_{cpu} \cdot \phi_{net}) + 0.005\Delta T \\ \frac{dT}{dt} = \frac{1}{C_{th}} i0.85p_{sys}(t) \_\_ hA(T \_\_ T_{amb})] \\ \frac{dSOH}{dt} = \_\_ 2.5 \times 10\_^{6} \cdot \left(\frac{p_{sys}}{p_{std}}\right)^{n} \cdot \exp\left(\_\_ \frac{50000}{RT}\right) \end{cases} \quad (29)$$

Based on the AndroWatts Mobile Energy Database, we obtained specific power consumption metrics for each usage scenario. From the NASA PCoE Battery Aging Dataset, we derived electrochemical parameters such as SEI impedance and capacity degradation coefficients, as is shown below:

Table 1: General parameters

Parameters	Value	Parameters	Value	Parameters	Value
Qremn	4Ah	ε	1.08	Vocv	3. 2 _ 4. 2V
$R_{\circ}$	0. 052	Rp	0. 032	pbase	0. 05W
I_{rf}	0. 4A	C,	800F	Δt	0. 1h

General parameters is shown in Table 1.

4.1.2 Method of SOC Model

We adopt the RK-4 method to solve this problem, pseudocode of which is as follows:

power coupling mechanism to predict the State of Charge (SOC). Algorithm 1: Battery Discharge Dynamics via Coupled RK-4 Solver

Note: This algorithm integrates the physical battery constraints with a non-linear

Input:

Initial state Soc0, T0, SoH0, Step size Δt, Time span tspan Scenario multipliers λscreen, λcpu, λnet.

Output:

Time series of SOC and Terminal Voltage vterm,

1:Initialize Soc = Soc0, T = T0, SoH = SoH0, and load battery coefficients. 2:While t < tspan and Soc > 0 do:

3: Step 1: Compute Slopes using 4th-order Runge-Kutta

4: k1 = DerivFunc(Soc, T, SoH)

5: k2 = DerivFunc(Soc + Δt/2. k1, T, SoH)

6: k3 = DerivFunc(Soc + Δt/2. k2, T, SoH)

7: k4 = DerivFunc(Soc + Δt. k3, T, SoH)

8: Step 2: Update State

9: Soc = Soc + Δt/6. (k1 + 2 * k2 + 2 * k3 + k4)

10: t = t + Δt

11:End While

12:Function DerivFunc(SOC, T, SOH)

13: psys = λscreen. pscreen + λcpu. pcpu + λnet. pnet //(Calculate coupled power)

14: Vocv = polyval(p, Soc) //OCV polynomial mapping

15: Ibat = f(psys, Vocv, R0) //Solve for (Current)

16:Return __ Ibat/(Qmax(T, SoH)) // SOC change rate

17:End Function

4.1.3 Results of SOC Model

Next, we obtained numerical solution via the RK-4 method above, and analyze battery performance under different usage scenarios and temperatures. The SOC variation and power consumption distribution of the mobile phone battery across various usage scenarios are shown in the figure 7:

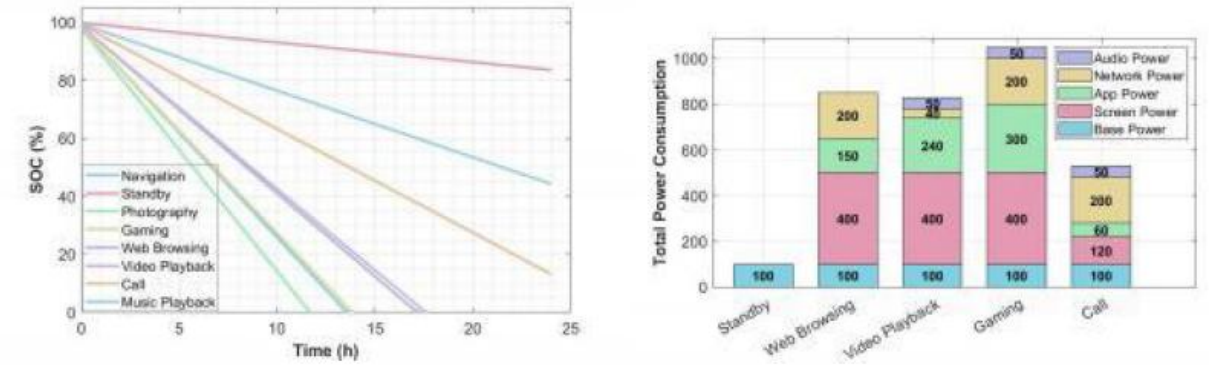

Figure 7: Scenario-based SOC decay & power breakdown

Scenario-based SOC decay & power breakdown is shown in Figure 7.

SOC trends and power distribution show scenario-specific discharge rates stem from distinct power compositions: gaming (highest power, fastest SOC drop) > web browsing/ video playback > standby (only basic power, slowest discharge), reflecting dynamic component power's direct impact on battery discharge.

Next, we analyzed SOC variations at different temperatures, as shown in the figure below:

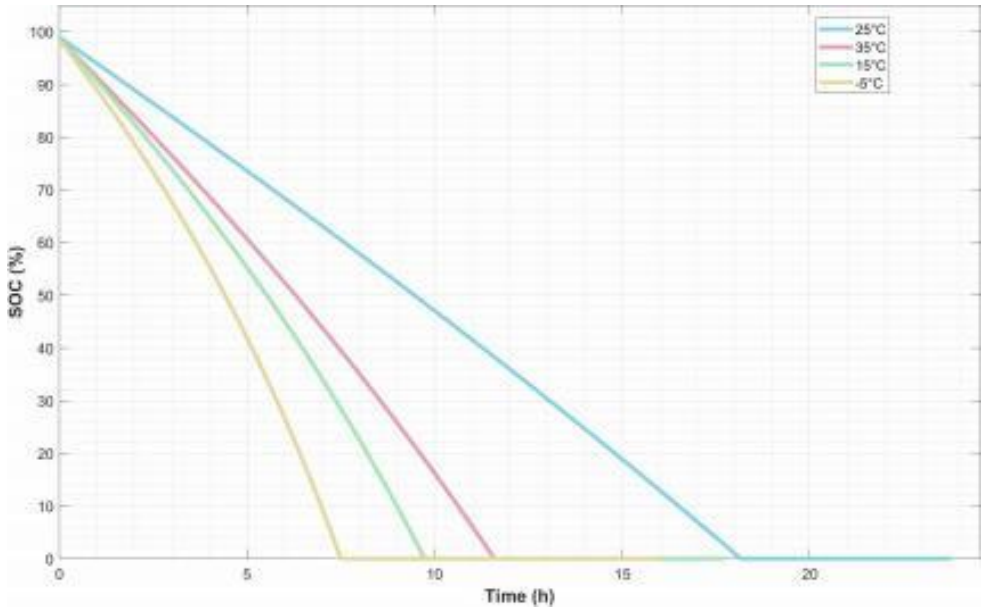

Figure 8: Relationship between SOC and temperature

Relationship between SOC and temperature is shown in Figure 8.

As shown in the figure above, battery performance decreases with falling temperatures, which is highly consistent with the measured results in the database.

4.2 Battery Depletion Prediction and Factor Analysis

4.2.1 Solution Formulas and Parameter Estimation

The core of this section is to accurately predict battery depletion time, quantitatively analyze the impact of various factors on battery life, and finally extract the optimal battery usage strategy.

The solution formulas directly adopt the battery depletion model and semi-physical factor impact model in Sections 3.1 and 3.2. The remaining battery life is obtained by iteratively solving the state space control equation with the fourth-order Runge-Kutta (RK4) method in Section 4.1, and the iteration terminates immediately when the terminal voltage drops to the preset cut-off threshold.

The core physical parameters of the model, especially SEI impedance and capacity degradation coefficients, are identified and calibrated using experimental aging data from the NASA PCoE database, with the specific parameter settings as follows:

Table 2: Parameters ofthe TTE prediction model

Parameters	Value	Parameters	Value
Qmax	4000mAh	V_0CP	3. 8V
ε	1. 2	Icrit	4000mA
k3	0. 12		

Parameters ofthe TTE prediction model is shown in Table 2.

4.2.2 Results of Time Prediction Model

We first predict battery depletion time across different usage scenarios via numerical integration, and conduct a comparative analysis of key indicators including power consumption and endurance performance, with the results as follows:

Data from the above figures and tables clearly shows significant differences in total power consumption and battery depletion time across scenarios: standby mode has the lowest power consumption and the longest depletion time, while gaming has the highest power consumption and the shortest depletion time. This fully validates that our power consumption model accurately depicts energy consumption laws in different scenarios.

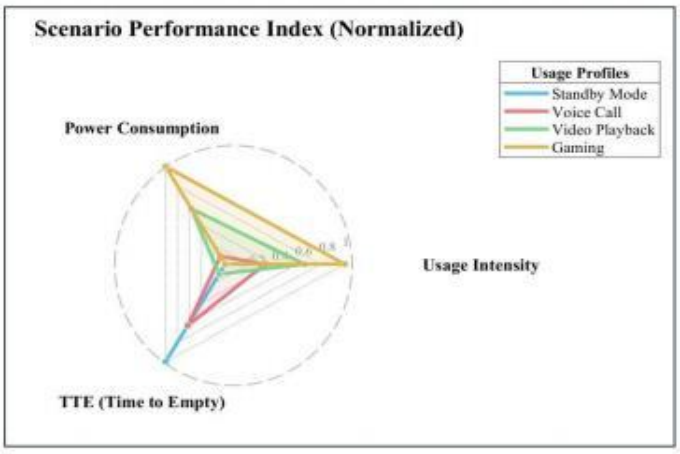

Figure 9: Radar chart for usage scenario comparison

Radar chart for usage scenario comparison is shown in Figure 9.

We also learn from literature that the initial battery health may affect depletion time. Based on endurance prediction results, we obtain the battery depletion time under different initial health levels and usage scenarios as follows:

Table 3: Table of TTE prediction results

Usage Scenario	Usage Intensity	Total Power Consumption (mW)	TTE(h)
Standby Mode	Almost No Use	125	32.8
Call	Light Use	265	15.1
Video Playback	Moderate Use	510	7.84
Gaming	Heavy Use	805	4.98

Table of TTE prediction results is shown in Table 3.

The data from the above figures and tables clearly shows significant differences in total power consumption and battery depletion time across scenarios: standby mode has the lowest power consumption and the longest depletion time, while gaming has the highest power consumption and the shortest depletion time. This fully validates that our power consumption model accurately depicts energy consumption laws in different scenarios.

We also learn from literature that the initial battery health may affect depletion time. Based on endurance prediction results, we obtain the battery depletion time under different initial health levels and usage scenarios as follows:

Table 4: Battery depletion results for different initial SOH

Initial SOH (%)	Standby Mode (h)	Video Playback (h)	Gaming (h)
100	33.5	8.05	4.98
80	26.7	6.4	3.95
60	19.8	4.75	2.9
40	13	3.1	1.85

Battery depletion results for different initial SOH is shown in Table 4.

As shown in the table, endurance time decreases with the drop in initial health, indicating that initial battery health is a key factor affecting phone endurance.

4.2.3 Multi-dimensional Impact Analysis

To identify the driving factors of rapid battery drain in different scenarios and the impact differences of parameters, this section conducted hardware state contribution decomposition experiments, parameter synergy effect tests, SOH decay model sensitivity analysis, and temperature- SOH evolution correlation experiments. The impacts of each variable were quantified from single- factor, multi-factor, and dynamic evolution dimensions, with results shown in Figure 10.

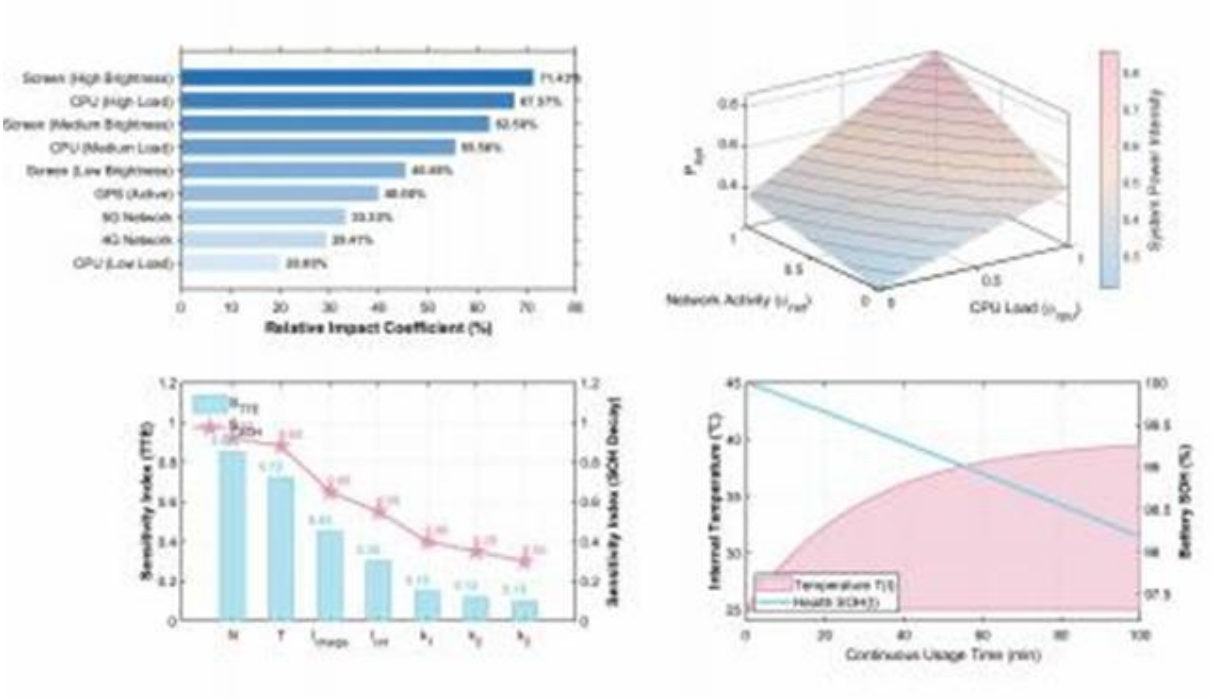

Figure 10: Multi-dimensional analysis of battery performance impacts

Multi-dimensional analysis of battery performance impacts is shown in Figure 10.

Overall, high screen load (e.g., high brightness + high refresh rate) is the primary driver of rapid battery drain across scenarios, and the synergy between CPU and network also significantly amplifies power consumption.

In high-load scenarios, hardware power consumption accelerates temperature rise, which in turn exacerbates battery SOH degradation, forming a positive feedback loop that is the core reason for rapid battery life reduction. The activities with the greatest impact on battery life are high screen brightness + high refresh rate combinations in high-load scenarios, and synergistic scenarios where both CPU and network are under high load.

In contrast, basic hardware activities such as GPS, low-load CPU, and standby states, as well as long-term slow degradation factors like calendar aging, have surprisingly small effects on short-term battery life.

5 Sensitivity Analysis

5.1 Sensitivity Analysis Under Different Usage Modes

To explore the dynamic changes of battery state and the coupling effects between parameters in real usage behavior, this section designs a stochastic scenario switching experiment (simulating users' irregular switching between standby, browsing, gaming and other scenarios). Meanwhile, the Monte Carlo method is introduced to perturb core parameters such as screen power and processor power. Finally, the SOC decay law under dynamic scenarios and the parameter interaction sensitivity results are obtained, as shown in Figure 11.

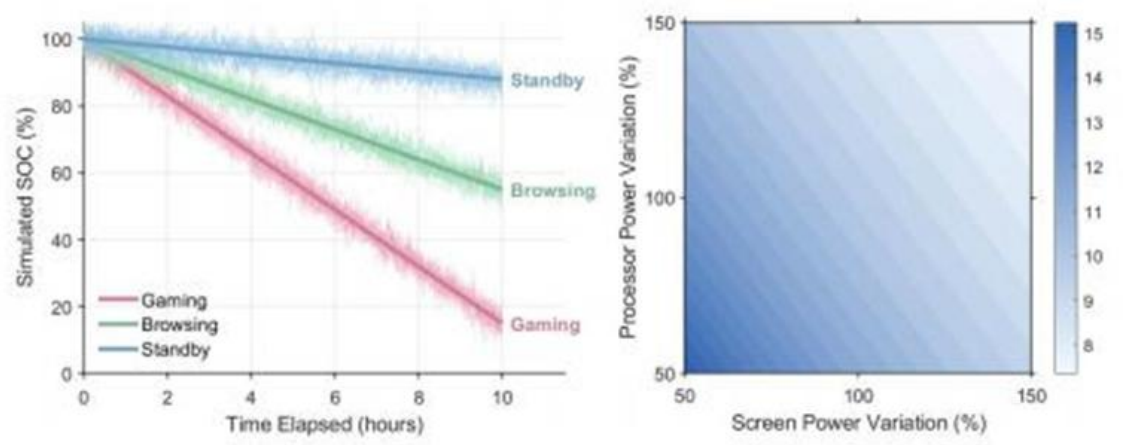

Figure 11: Sensitivity analysis under different usage modes Sensitivity analysis under different usage modes is shown in Figure 11.

It can be observed from the figure that the SOC decay rate in the gaming scenario is significantly higher than that in standby and browsing scenarios. In the heatmap, the interaction effect between screen power and processor power (indicated by color depth) has a more significant impact on battery performance than other parameter combinations, which indicates that the synergistic changes of core hardware power in high-load modes are the key factors affecting battery life.

5.2 Sensitivity Analysis of Each Parameter

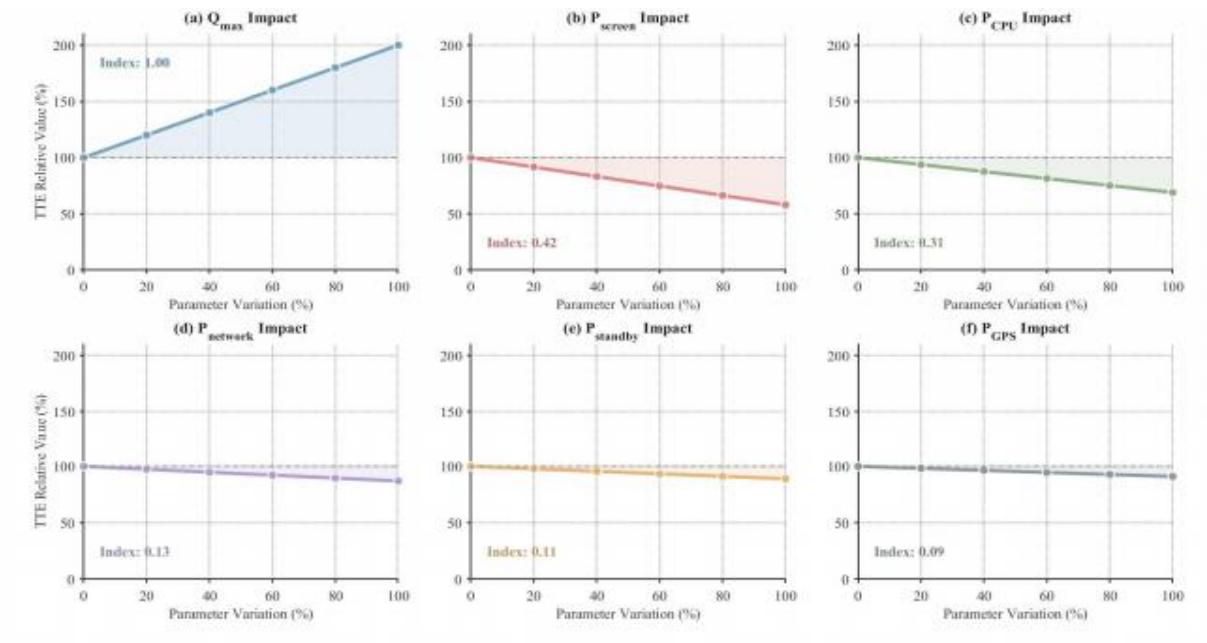

Figure 12: Sensitivity analysis of each parameter

Sensitivity analysis of each parameter is shown in Figure 12.

To quantify the impact of key parameters on Time to Empty (TTE), single-factor perturbation experiments (0- 100% variation) are conducted on battery capacity, screen power, etc., based on Section 3.1 TTE sub-model, yielding each parameter's sensitivity curve. For

streaming scenarios, multi-factor coupling experiments (temperature & screen brightness synergy) are designed to test battery life, with results in Figs. 12 & 13.

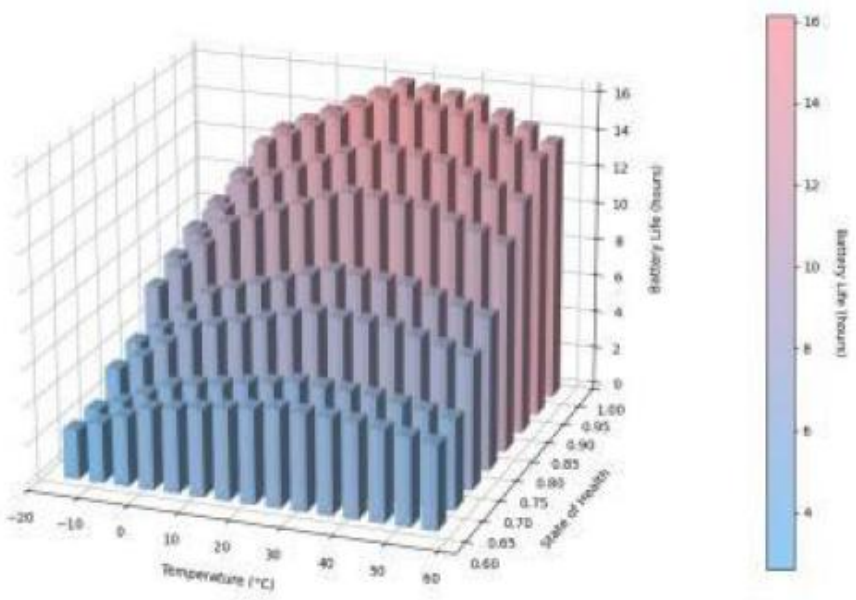

Figure 13: Temperature-SOH sensitivity analysis

Temperature-SOH sensitivity analysis is shown in Figure 13.

Battery capacity most affects TTE, temperature and screen brightness together shorten streaming scenario battery life (especially over 40°C), so both need constraining in high-load cases.

5.3 Sensitivity Analysis Under Different Assumptions

We categorized the model hypotheses into three parts: the base model, the temperature-coupled model, and the model coupling both temperature and aging. By comparing these hypotheses, we obtained the sensitivity analysis results under these three different assumptions:

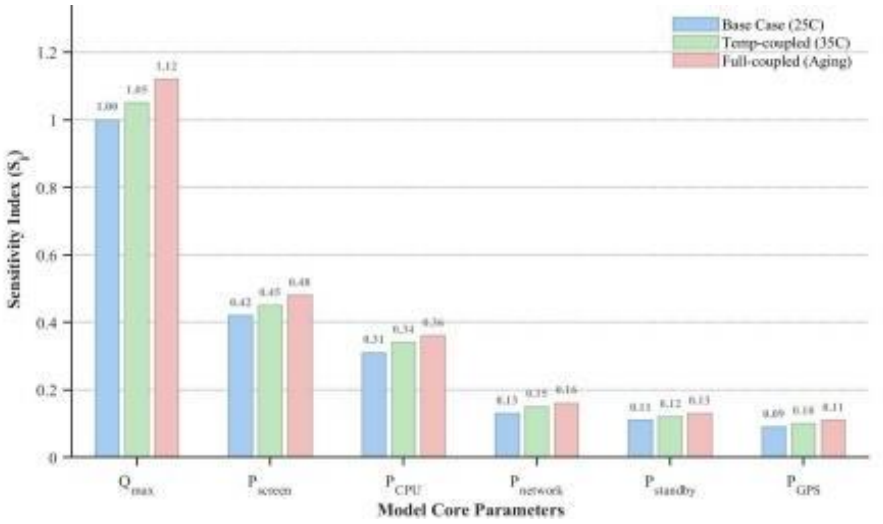

Figure 14: Sensitivity analysis under different assumptions

Sensitivity analysis under different assumptions is shown in Figure 14.

It can be seen that under the hypothesis coupling both temperature and aging, the sensitivity of each parameter to the model is generally higher than that of the base model, with the sensitivity of battery capacity increasing most significantly.

6 Conclusions

By constructing a state-space model that couples multiple physical fields, this paper systematically investigates the state evolution of smartphone batteries under complex load conditions, achieving cross-scale modeling from transient state-of-charge estimation to long-term battery life prediction. The study not only reveals the decisive role of high brightness, high refresh rates, and processor-network collaboration in rapid battery depletion but also quantifies the nonlinear interference of ambient temperature and aging state on battery internal resistance and effective capacity. Experimental validation demonstrates that the model exhibits good robustness and adaptability to various dynamically switching usage scenarios. However, due to the model's reliance on iterative solutions to complex nonlinear equations and high-resolution sensitivity mapping, its real-time computational overhead on low-power hardware is relatively high. Future research will focus on optimizing the algorithm's computational efficiency to support real-time operation in embedded systems, and will explore extending this multi-physics coupling framework to various portable electronic devices—such as drones and smartwatches—that have stringent energy management requirements.

References

[1] González D F, Peris H D, Orpinell B G, et al. Modeling and impact assessment of hybrid battery –supercapacitor energy storage solutions for electric vehicles[J]. Journal of Energy Storage, 2026, 152(PC): 120811.

[2] Li X, Yu D, Vilsen B S, et al. Degradation analysis and tanks-in-series modeling of lithium-ion batteries with state of health-adaptive charging strategies[J]. eTransportation, 2026, 100561.

[3] Bavithra R, Jaya J. Hybrid Optimization and Deep Graph-GRU Based Energy-Efficient Routing and Fault Prediction in WSNs for Smart Agriculture Applications[J]. Iranian Journal of Science and Technology, Transactions of Electrical Engineering, 2026, (prepublish): 1-29.

[4] Khekare U, S. I V R. LHO _HLiB: Hybrid Lithium Battery Management System for Effective Charge – Discharge Management in Electric Vehicles[J]. Energy Technology, 2026, 14(1): e202501015.

[5] Gopal K R, Ma B, Bai P. Mapping Out Fast Charging Safe Limits for High-Loading Lithium- Ion Cells by High-Fidelity Operando Microscopy.[J]. Small (Weinheim an der Bergstrasse, Germany), 2026, e14619.

[6] Liu S, Li Y, Li S. Effective anode protection for zinc-ion batteries using a covalent – organic framework coating strategy[J]. Electrochimica Acta, 2026, 148191.

[7] Radhakrishnan A, Prasad V R, Railis J D, et al. Enhancing thermal management in electric vehicles to improve performance and extend battery life using advanced cooling systems[J]. Journal of Thermal Analysis and Calorimetry, 2026, (prepublish): 1-20.

[8] Zhang Y, Sun Z, Cai C. Real-time adaptive hybrid energy management for hybrid-electric UAVs: Offline – online DP-ECMS collaborative strategy in low-altitude inspection[J]. Franklin Open, 2026, 100473.

[9] Samal B K, Pati S, Sharma R. Power management using an improved EMS algorithm in a stand-alone hybrid PV-PEMFC microgrid with reduced converter count[J]. Green Energy and Intelligent Transportation, 2026, 5(2): 100302.

[10] Huang K, Zhang X, Guo Y, et al. Source domain selection with early-cycle features for transfer learning-based prediction of lithium-ion battery degradation trajectories[J]. Energy, 2026, 139928.

[11] Jiang Z, Yang J. Optimization of UAV Smoke Screen Jamming Bomb Deployment Strategy and Collaborative Effect Study[J]. Academic Journal of Computing & Information Science, 2025, 8(10).

[12] Kharade A P, Mohite B R, Janardhanan J, et al. Improving the charging system and battery health of electric vehicles using AC –DC power factor correction resonant converters[J]. Electrical Engineering, 2026, 108(2): 121.

[13] Mijailovic S A, Gan C, Sheldon W B. Scaling Models for Coupled Intercalation Dynamics, Electrolyte Depletion, and Lithium Plating during Fast Charging[J]. Journal of The Electrochemical Society, 2026, 173(1): 010507.

[14] Shin G, Kang J. Data _Driven Machine Learning Model for Battery Life Prediction Across Electrode Materials[J]. International Journal of Energy Research, 2026, 2026(1): 8083561.

[15] Xie Y, Ding J, Li W, et al. An improved thermal control strategy for raising energy efficiency and battery life in electric vehicles[J]. Energy, 2026, 139806.

[16] Aranizadeh A, Vahidi B, Khorsandi A. Extending battery health in wind-integrated systems through optimal state of charge management: A multi-objective approach[J]. Journal of Energy Storage, 2026, 119980.

[17] Li X, Zhang H, Liu C, et al. Hierarchical real-time energy management strategy of eVTOL hybrid power system based on finite-set[J]. Aerospace Science and Technology, 2026, 111546.

[18] Kavasoğullari B, Karagöz E M. Numerical study on the heat transfer enhancement and fin size optimization of hybrid battery thermal management system[J]. Physica Scripta, 2026, 101(1): 015209.

[19] Park S E, Liu X, Hwang J H, et al. Deep Convolutional Neural Network-Based Detection of Gait Abnormalities in Parkinson's Disease Using Fewer Plantar Sensors in a Smart Insole[J]. Biosensors, 2026, 16(1): 40.

[20] Zhou W, Li B, Zeng X. Intrusion detection model ofUAV system based on machine learning and neural network[J]. Frontiers in Physics, 2026, 1660104.